



Soil–Geosynthetic Interaction Under Triaxial Conditions: Shear Strength Increase and Influence of the Specimen Dimensions

Rafael Anjos¹ · David Miranda Carlos¹ · Sónia Gouveia^{2,3} · Margarida Pinho-Lopes¹ · William Powrie⁴

Received: 29 July 2023 / Accepted: 30 October 2023 / Published online: 14 November 2023
© The Author(s) 2023

Abstract

Geosynthetics are extensible reinforcements used to enhance the engineering performance of a soil. The transfer of stresses from the soil to the reinforcement is achieved through soil–geosynthetic interaction. The proposals from the literature to assess the shear strength of the reinforced soil under triaxial conditions use three different approaches. These involve analysing the reinforced soil: (i) as a homogeneous composite material (Approach A), (ii) as two different materials (Approach B), or (iii) as soil having the same fundamental shear strength, with the effect of the reinforcement represented as an additional lateral or confining stress (Approach C). In this paper, triaxial tests data of a soil reinforced with a geosynthetic, and specimens with different dimensions (diameters 70 and 150 mm) were used to assess changes in shear strength and to carry out a statistical analysis. The increases in shear strength of the reinforced soil and of the soil–geosynthetic interface were analysed using equations from the literature. The difference between the triaxial results obtained from specimens of different sizes was assessed using an Analysis of Covariance (ANCOVA). When the joint term of the regression model was not statistically significant, the characterisation from different specimen sizes was used to generate soil failure envelopes. Thus, a new methodology to obtain a failure envelope with different specimen sizes is presented.

Keywords Triaxial tests · Granular soil · Dimension of specimens · Geosynthetics · Statistical analysis

Background

Geosynthetics are extensible reinforcements used to enhance the engineering performance of a soil. The transfer of stresses from the soil to the reinforcement is achieved through soil–geosynthetic interaction. Assessment of the strength and stiffness of reinforced soil is crucial in the design of geotechnical structures adopting this approach. In reinforced soil walls, the introduction of geosynthetics provides additional load resistance through two mechanisms [1]: friction along the soil–geosynthetic interface and, for geogrids, passive resistance along its transverse members. The applications of geosynthetics in roadways and railways, particularly stabilising soil, may involve loading conditions close to axisymmetric; in reinforced soil structures with a main direction of loading, loading tends to occur in plane strain conditions. Regardless of the type of structure and reinforcing mechanism mobilised, the soil–geosynthetic interface strength is key for the design of structures in soil reinforced with geosynthetics.

For drained conditions, this strength is often represented using a Mohr–Coulomb model [2] or a factor representing

✉ Margarida Pinho-Lopes
mlopes@ua.pt

Rafael Anjos
rafaelanj@ua.pt

David Miranda Carlos
dmc@ua.pt

Sónia Gouveia
sonia.gouveia@ua.pt

William Powrie
W.Powrie@soton.ac.uk

¹ Department of Civil Engineering, RISCO, University of Aveiro, Aveiro, Portugal

² Institute of Electronics and Informatics Engineering of Aveiro (IEETA) and Department of Electronics, Telecommunication and Informatics (DETI), University of Aveiro, Aveiro, Portugal

³ Intelligent Systems Associate Laboratory (LASI), Porto, Portugal

⁴ School of Engineering, University of Southampton, Southampton, UK

the efficiency of the interface relative to the shear strength of the soil, R_{int} . This interface efficiency factor can be defined as

$$R_{\text{int}} = \frac{a' + \tan\delta}{c' + \tan\phi'}, \quad (1)$$

where δ is the friction angle and a' is the adhesion of the soil–geosynthetic interface, ϕ' the friction angle of the soil, and c' an effective cohesion. The R_{int} formulation (Eq. 1) is flawed by the inclusion of an effective cohesive intercept, c' , for the response of the soil, and of an adhesion, a' , for the soil–geosynthetic interface, that have no physical meaning for most natural soils. Thus, Eq. 1 should be rewritten as

$$R_{\text{int}} = \frac{\tan\delta}{\tan\phi'}. \quad (2)$$

The R_{int} factor typically ranges between 0.6 and 1.0 [3], where lower values are typical of geotextiles and values higher than 1 can occur for geogrids, owing to the additional strength mobilised due to the passive resistance on its transverse ribs.

Soil–geosynthetic interaction depends on the type of geosynthetic. Planar geosynthetics mobilise frictional resistance along the contact surfaces with soil. Geogrids, in addition, mobilise passive resistance through contact between soil particles and the geogrid ribs when there is movement of the reinforcement relative to the soil. As soil particles enter the geogrid openings, they interlock with neighbouring grains and propagate this effect through a certain height, leading to stabilisation [4]. The interface strength is often measured as a friction angle on the soil–geosynthetic interface, δ . Different laboratory tests can be used to assess the soil–geosynthetic interface strength, depending on the relative movement analysed. Examples include direct shear tests and pull-out tests. The equipment used to assess the soil–geosynthetic interaction must be large enough to provide realistic results, and therefore involves large volumes of soil and significant periods of time for preparation and disassembly. It is of merit to find a methodology to assess the friction angle of the soil–geosynthetic interface through triaxial tests. The validation or implementation of this methodology will enable the characterisation of reinforced soil using procedures commonly used to assess the shear strength of unreinforced soils.

Among other factors, the shear strength of reinforced soil depends on the shear strength mobilised in the soil and on the tensile stress in the reinforcement. The deformation and stiffness of both soil and reinforcement influence the relative values of these components of strength [3]. Two reinforcement mechanisms have been identified in triaxial tests on reinforced soil (Saez [5] cited by Carlos et al. [6]): (i) tensile forces in the reinforcement and (ii) frictional forces at the

soil–reinforcement interface. The first mechanism is limited by the tensile strength of the reinforcement, whereas the second depends on the magnitude of relative displacements between soil and reinforcement and is limited by the shear strength of the soil–reinforcement interface. In triaxial tests, tensile failure of the reinforcement layer is uncommon [6] and failure is more frequently by slippage of the soil with respect to the reinforcement, resulting in bulging between layers [7].

In the literature, there are different approaches to estimate the shear strength of frictional reinforced soil and its increase relative to the unreinforced soil strength based on results from triaxial tests. These involve analysing the reinforced soil (i) as a homogeneous composite material (Approach A), (ii) as two different materials (Approach B), or (iii) as soil having the same fundamental shear strength, with the effect of the reinforcement represented as an additional lateral or confining stress (Approach C). The composite material approach (Approach A) often uses an apparent cohesion (c'_r) [8] (Fig. 1a), or an apparent friction angle (ϕ'_r) [9] (Fig. 1b), both equivalent to an additional lateral confining stress ($\Delta\sigma'_3$) acting along the full height of the specimen [7]. When the effect of the reinforcement is considered separately (Approach B), a friction angle of the soil–geosynthetic interface δ is considered [10]. In Fig. 1c, the reinforcement effect is represented as an additional lateral confining stress ($\Delta\sigma'_3$), assuming the shear strength is the same as that of the unreinforced soil (ϕ') (Approach C). In Fig. 1, τ is the shear stress, σ' is the normal stress, σ'_{3fU} is the confining stress at failure of the unreinforced soil, σ'_{1fU} is the major principal stress at failure for the unreinforced soil, σ'_{1fR} is the major principal stress at failure for the reinforced soil, and $\Delta\sigma'_{1fR-U}$ is the increase in the major principal stress of reinforced soil relative to the unreinforced soil. This relation can be expressed numerically as

$$\Delta\sigma'_{1fR-U} = \sigma'_{1fR} - \sigma'_{1fU}. \quad (3)$$

Gray et al. [7] review some proposals in the literature for quantifying the strength increase due to reinforcement of soil with geosynthetics. As an example, for a horizontal layer of reinforcement, Schlosser and Long [8] suggest that c'_r (Approach A) can be estimated as

$$c'_r = \frac{\alpha_F \sqrt{K_p}}{2h_{vr}} \quad (4)$$

$$K_p = \left(\tan \left(45^\circ + \frac{\phi'}{2} \right) \right)^2, \quad (5)$$

where α_F is the force per unit width of reinforcement at failure, K_p is the passive lateral earth pressure, and h_{vr} is the vertical spacing between adjacent reinforcement layers.

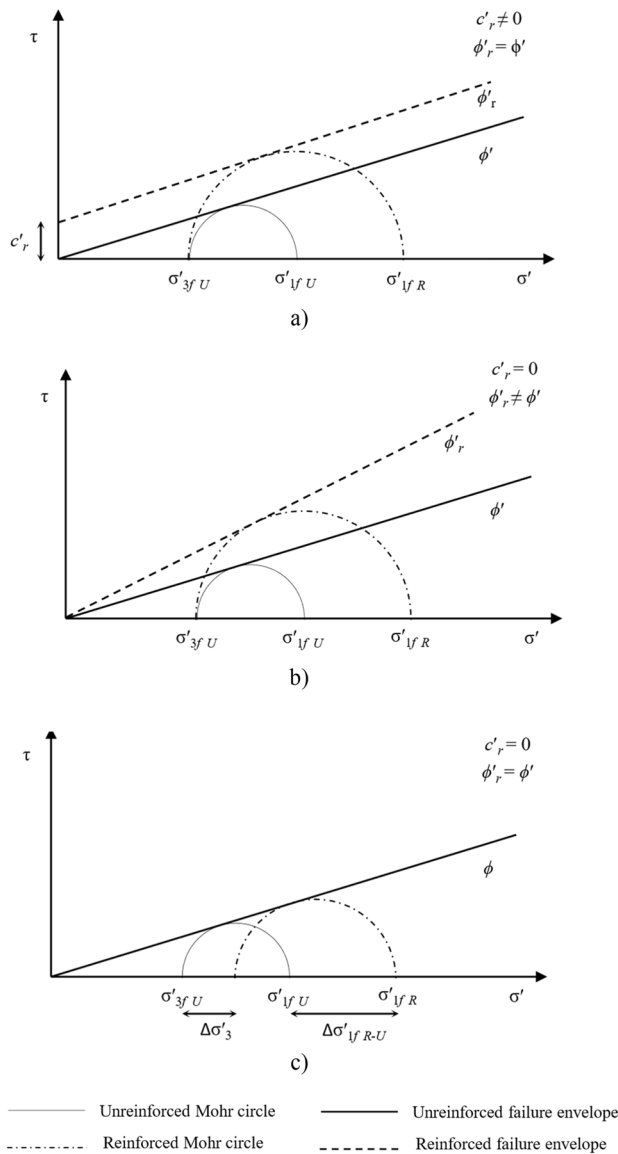


Fig. 1 Conceptual models for frictional (non-cohesive) soils proposed in the literature used to represent the increase in shear strength of reinforced soils based on results from triaxial test: **a** apparent cohesion; Approach A (adapted from [10]); **b** apparent friction angle; Approach A; **c** additional lateral confining stress; Approach C (adapted from [10])

Furthermore, $\Delta\sigma'_3$ (Approach C) is quantified from α_F and h_{vr} as

$$\Delta\sigma'_3 = \frac{\alpha_F}{h_{vr}} \tag{6}$$

Gray et al. [7] suggest an alternative form for c'_r (Approach A) depending explicitly on $\Delta\sigma'_3$ (Approach C) as

$$c'_r = \frac{\Delta\sigma'_3 \sqrt{K_p}}{2} \tag{7}$$

$$\Delta\sigma'_3 = \sigma'_{3fU} \left(\frac{\Delta\sigma'_{1fR-U}}{\sigma'_{1fU}} \right) \tag{8}$$

The additional lateral confining stress (Approach C) is then obtained based on similarity of triangles (Fig. 1c). Alternatively, Yang [11] cited by Gray et al. [7], states that the additional lateral confining stress can be estimated by Eq. 9, based on the Mohr–Coulomb formulation from

$$\sigma'_{1fR} = (\sigma'_{3fU} + \Delta\sigma'_3) K_p \tag{9}$$

Higuchi et al. [9] report results from soil reinforced with geosynthetics tested under plane strain conditions. Bulging and lateral deformation of the specimens occur under axial loading, mobilising tensile stresses in the reinforcement. Such forces and their effect on the overall response is represented by an additional lateral confining stress $\Delta\sigma'_3$ (Approach C). Higuchi et al. [9] propose quantifying this additional lateral confining stress as a peak friction angle for the composite material, ϕ'_r (Approach A), using

$$\phi'_r = \sin^{-1} \frac{\left(\frac{\sigma'_{1fR}}{\sigma'_{3fR}} \right) - 1}{\left(\frac{\sigma'_{1fR}}{\sigma'_{3fR}} \right) + 1} \tag{10}$$

These methodologies reported for representing the effect of the reinforcement by means of Approach A using an apparent cohesion (Eqs. 4 and 7) or an apparent friction angle (Eq. 10) have their merits. However, from a geomaterial and geotechnical point of view, it is known that the introduction of a reinforcement layer does not generate cohesion between soil particles (i.e., there is no cementation) and does not change the friction angle of the soil. The soil below and above the reinforcement layer will still be characterised by its native friction angle, particularly at critical state. It is therefore erroneous to represent the reinforcement effect by means of non-existent cohesive or frictional resistance. Often, when this type of methodology is disseminated, the concept of cohesion and soil friction angle are misunderstood. Analysing results from triaxial tests on both unreinforced and reinforced soil, with geosynthetics, Ruiken et al. [12] propose to only use the concept of additional lateral confining stress (Approach C) to explain the increase in shear strength when reinforcement layers are introduced in a soil (Fig. 2). This additional confining stress is, once again, explained by the relative displacement between soil

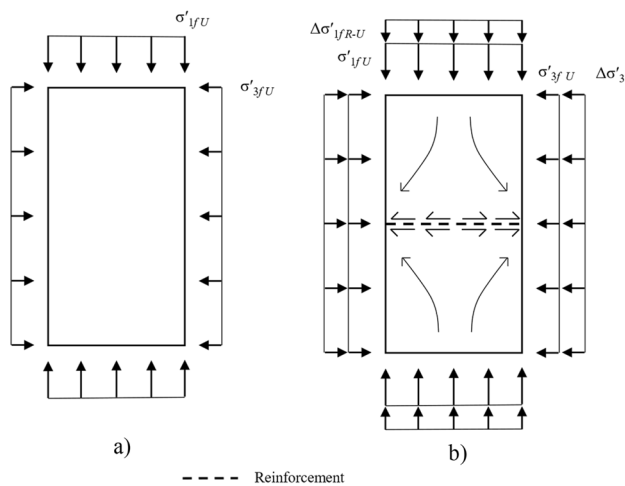


Fig. 2 Confining stress increase concept, major principal stresses (Approach C): **a** major principal stresses for the unreinforced soil; **b** major principal stresses for the reinforced soil (adapted from [12])

and reinforcement induced by loading of the specimen, which in turn causes an increase of the frictional force at the reinforcement level, up to a limit.

The additional confining stress at failure (Approach C) is quantified by Markou [13] using Eq. 8. To relate the additional lateral confining stress (Fig. 2) to the friction angle of soil–geosynthetic interface, Markou [13] adopts the formulation propose by Atmatzidis et al. [14] to estimate δ (Approach B) as

$$\tan\delta = \frac{\Delta\sigma'_3}{\sigma'_{1R}} \frac{3H}{2R_0}. \quad (11)$$

Here, H is the overall height of the specimen and R_0 is the reinforcement disc radius; the additional lateral confining stress $\Delta\sigma'_3$ is obtained from Eq. 8. Equation 11 assumes that the shear strength at the interface is not fully mobilised along the radius of the reinforcement disc [15]. The mobilised shear strength varies linearly along the radius of the reinforcement element and the normal stress at failure on the interface at the perimeter of the reinforcement is equal to the major principal stress at failure, σ'_{1FR} .

Equation 11 gives δ as a function of the additional lateral confining stress, which may be obtained from Eq. 8 or Eq. 9. There is no justification in the literature for using the latter rather than Eq. 8. For this reason, in this paper, both equations are implemented to quantify the variation in shear strength observed when including a disc of geosynthetic reinforcement in a soil, subjected to a triaxial test.

Another important consideration is the sample size [16]. Usually, specimens for triaxial tests are cylindrical and have a height that is twice the diameter. The minimum dimensions of the specimen are governed by the maximum size of the

soil particles, and the specimen diameter should be at least six times the largest particle size for uniformly graded material and eight times for well-graded material [17]. According to BS EN ISO 17892-8 [18], the maximum particle size to use in a triaxial specimen should not exceed 1/6 of the specimen diameter. This is the criterion for selecting the specimen size for unreinforced soil. For reinforced soil, there is no specific rule. Some authors adopt the same minimum size as for the unreinforced specimens, while others select the largest possible specimen size that the equipment will hold. The dimensions of the geosynthetic and characteristics of soils, such as fabric and structure, all influence the response of reinforced soil; thus, using large enough specimens tends to increase representativeness of the specimen of the true bulk behaviour of the material [16, 17]. However, for reasons of economy and time, small specimens are more often used to characterise soils and reinforced soils.

Markou and Droudakis [19] report triaxial test results for sand reinforced with 3, 5, or 7 layers of geotextiles for different specimen sizes (diameters of 50 mm and 70 mm). The shear strength increases by adding the reinforcement layers, more importantly for a higher number of reinforcement layers and cell pressure. Larger specimen sizes and an increasing number of reinforcement layers lead to an increase in the axial strain at failure. An empirical equation for quantifying the additional lateral confining stress representing the effect of the reinforcement is proposed, considering the specimen size, number of reinforcement layers, and cell pressure. The equation involves empirical constants, calibrated for the results obtained by the authors (soil, reinforcements, and testing conditions). The proposed equation includes the spacing between consecutive layers of reinforcement and cannot be applied to test specimens having a single layer of reinforcement.

One of the major problems in geotechnical engineering is the limited availability of data, which impacts on quantifying the statistical accuracy of the measurements. For example, when estimating the shear strength of a soil using Mohr circles (or alternative, equivalent quantities), the failure envelope is obtained using a minimum of three sets of data (or points). Experimental results are often compared based on sample estimates and conclusions are drawn without adequate statistical support, which may be misleading with respect to the expected response of the soil (population). This paper explores that problem and presents an innovative methodology to assess the statistical similarity between results obtained from specimens of different sizes of unreinforced and reinforced soils. Some guidelines for testing reinforced soil specimens and a novel methodology to generate failure envelopes with results from specimens of different sizes are proposed.

Three or more triaxial tests carried out at different confining stresses are required to determine the strength parameters

of the soil. Each test results in a Mohr circle with the failure envelope generally represented as the line that forms the common tangent to all three Mohr circles. The failure envelope is commonly described by the equation of a straight line

$$\tau = \pm(c' + \sigma' \tan \phi') \quad (12)$$

with parameters c' (intercept), $\tan \phi'$ (slope). As already mentioned, this approach has serious limitations as it does not represent the real shapes of the failure envelopes of soils in a Mohr diagram in terms of either peak or critical states (Fig. 3). The peak failure envelope is linear at high confining stresses and curved at low confining stresses, with no real cohesive strength. The critical state failure envelope is linear, with no cohesive strength component.

The selection of the best-fit failure envelope forming the common tangent to all Mohr circles becomes more difficult as the number of tests carried out at different confining pressure increases. This task can be simplified if each Mohr circle is represented as a point in a different set of coordinates (s', t) plotted in a $s' t$ diagram (Eqs. 13 and 14, respectively). Then, a linear regression can be fitted to those points

$$s' = \frac{\sigma'_1 + \sigma'_3}{2} \quad (13)$$

$$t = \pm \frac{\sigma'_1 - \sigma'_3}{2}, \quad (14)$$

where σ'_1 is the major principal stress, σ'_3 is the minor principal stress (in the case of a conventional triaxial test it is the confining stress), s' is the centre and t is the radius of the Mohr circle. The sign of t depends on the angle of the major principal stress with the horizontal: if the angle is greater than or equal to 45° , $t > 0$; otherwise, $t < 0$. Then, a linear regression can be fitted to those points. Mathematically, this process is a Linear Regression Analysis (LRA), and it is

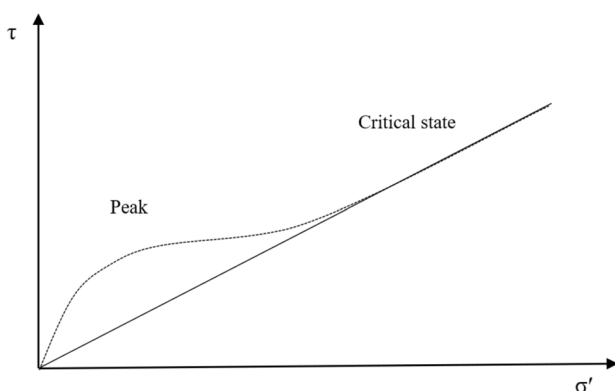


Fig. 3 Typical Mohr diagram at peak and critical state

used to study the effect of X (dependent variable) on a quantitative variable (Y , response), where Y is a linear function of X [20]. This is a common approach in geotechnical engineering; however, it must be pointed out that s' and t result from the dependent (σ'_1) and independent (σ'_3) variables.

The LRA is based on a (random) sample of observations from the population targeted in this study. Intuitively, the results on a sample would be expected to be closer (on average) to those of the underlying population as the sample size increases. However, the LRA carried out in geotechnical engineering usually disregards the process of statistical inference, i.e., the extrapolation of the conclusions conveyed in the analysis of the sample to the population.

This paper focuses on the soil geosynthetic interface shear strength under triaxial conditions. The applications of geosynthetics targeted include transportation infrastructure, where the loading is closely axisymmetric. Results from previous triaxial tests on different sized specimens are analysed to assess the soil–geosynthetic interface strength using equations from the literature. Differences between the triaxial results obtained from specimens of different sizes is assessed using an Analysis of Covariance (ANCOVA).

Materials and Methods

In the following sections the materials and methods are described. Section 2.1 provides an overview of the experimental procedure, including the characterisation of the soil, the setting up of the triaxial tests, and the approaches to quantifying the effect of the reinforcement on the shear strength of the soil. Section 2.2 presents the procedures used in the statistical analysis.

Experimental Procedure and Shear Strength Analysis

This study uses data from the triaxial tests presented in Carlos et al. [6] and Carlos [21], on a residual soil derived from granite consisting of poorly graded sand made up of 8% fines, 60% sand sized particles, and 32% gravel, classified as SW-SM according to the Unified Soil Classification System [22]. The soil maximum particle size is 12.7 mm and the representative particle sizes for 10% and 50% are, respectively, 0.084 and 1.000 mm. The coefficient of uniformity and of curvature are, respectively, 16.7 and 0.9. Figure 4 shows the soil particle-size distribution. The maximum void ratio is 1.00 and the minimum 0.48. The specific gravity of the soil particles is 2.55. Figure 5 shows the geocomposite used to reinforce the specimens. It consists of a geotextile backing (continuous filament, non-woven) reinforced by high tenacity polyester yarns. The geocomposite has a mass per unit area of 325 g/m^2 . The tensile strength and corresponding strain are, respectively,

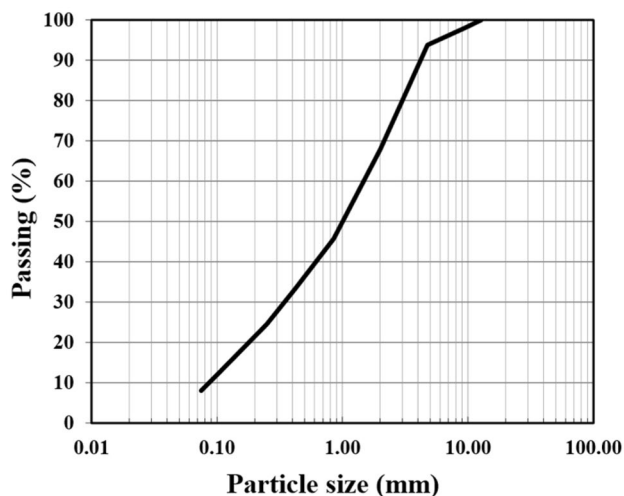


Fig. 4 Particle-size distribution of the soil studied

54.6 kN/m and 10.6% in the machine direction, and in the cross-machine direction 15.6 kN/m and 79.9%. The geocomposite studied is orthotropic, along its machine and cross-machine directions (as are most geosynthetics), and thus, an average response is obtained in the triaxial tests. The geosynthetic chosen is a continuous material (without openings that would mobilise different interaction mechanisms, i.e., interlocking), and combines the functions of separation, filtration, and reinforcement, typical of transportation infrastructure.

As previously stated (Sect. 1), larger triaxial specimens are preferable. However, small specimens are used in practice to allow for feasible testing times and affordable costs. In this study, the specimen size for unreinforced soil was chosen to comply with the current literature indications, i.e., with a diameter of at least six times the largest particle size for uniformly graded soil [18]. Without any specific rule to choose the size of the reinforced soil specimens, the same rationale used for the unreinforced specimens was

adopted. In this work, the maximum soil particle size was $D_{max} = 12.7$ mm implying that the specimen diameter for testing should be at least of 76.2 mm (i.e., 6 times larger than D_{max} , Table 1). According to BS EN ISO 17892-8 [18], the maximum particle size in a triaxial specimen should not exceed 1/6 of the specimen diameter. In this paper, the smaller triaxial specimens had a diameter of 70 mm, and thus, the corresponding maximum particle size is 11.67 mm. The soil considered had 1.93% of particles with sizes ranging between 9.51 mm (3/8") and 12.7 mm (1/2"). Therefore, the larger particles were neglected (very low occurrence) and were not removed before testing. For the largest triaxial specimens (150 mm diameter), the corresponding maximum particle size is 25 mm.

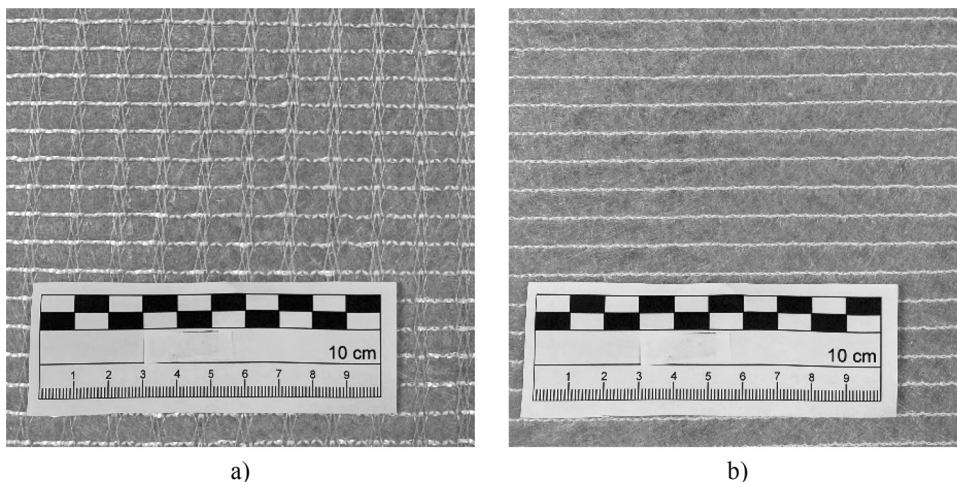
This study considers two sets of cylindrical specimens (Table 1) with different diameters, D , and heights, H : (i) $D = 70$ mm and $H = 140$ mm, specimens denoted by $D70$; and (ii) $D = 150$ mm and $H = 300$ mm, denoted by $D150$. The results obtained using the smaller specimens were validated against specimens of 150 mm diameter, which according to the $6 \times D_{max}$ rule are of adequate size for the soil used. Reinforcement (denoted by R) was included as a disc of geocomposite (diameter $\sim D$) placed horizontally at the mid-height of the specimen ($H/2$), always with the

Table 1 Nomenclature adopted and specimen layout (dimensions and location of the reinforcement layer) for the triaxial tests

| Nomenclature | Diameter, D (mm) | Height, $H = 2D$ (mm) | Reinforcement location (mm) | Number of specimens tested |
|--------------|--------------------|-----------------------|-----------------------------|----------------------------|
| $UD70$ | 70 | 140 | – | 9 |
| $UD150$ | 150 | 300 | – | 3 |
| $RD70$ | 70 | 140 | $H/2 = 70$ | 9 |
| $RD150$ | 150 | 300 | $H/2 = 150$ | 3 |

All specimens were analysed at two different states: peak stress ratio and at the end of the test (17% axial strain)

Fig. 5 Geocomposite a lower face; b upper face



lower face (identified in Fig. 5a) towards the base cap of the specimen. All specimens were prepared similarly by compaction to a relative density of 83%, and tested dry at a strain rate of 0.7% per minute at a confining stress of 50, 100, or 150 kPa. More details on specimen preparation can be found in Carlos et al. [6]. The results of the unconsolidated undrained triaxial tests were analysed according to BS EN ISO 17892-8 [18]. Some tests were repeated in the same experimental conditions to evaluate the reproducibility of the results and to enable a more robust statistical analysis; three different *D70* specimens were tested at each confining stress (50, 100, and 150 kPa), and one *D150* specimen was tested for each confining stress, totalling 24 (12 *U* and 12 *R*) observations. Table 1 summarises the nomenclature adopted for the different specimens considered in this work. Tests were terminated at an axial strain of 17%, and there was no clear evidence of specimens reaching a critical state. Accordingly, the results are reported at the peak stress ratio and at the end of the test, at an axial strain of 17%.

The triaxial test results were analysed using the conventional method, estimating the mobilised angle of friction ϕ'_{mob} (Eq. 15), the triaxial shear strain ϵ_s (Eq. 16), the three-dimensional stress invariants, the deviator stress q (Eq. 17), and the mean effective stress p' (Eq. 18). According to Wood [23], q and p' are the appropriate stress parameters to use for the axisymmetric conditions of the triaxial test. The ratio (t/s') is implicit in Eq. 15, used to determine ϕ'_{mob}

$$\phi'_{\text{mob}} = \sin^{-1} \left(\frac{\sigma'_1 - \sigma'_3}{\sigma'_1 + \sigma'_3} \right) = \sin^{-1} \left(\frac{t}{s'} \right) \tag{15}$$

$$\epsilon_s = \frac{2}{3} (\epsilon_a - \epsilon_r) \tag{16}$$

$$q = \sigma'_1 - \sigma'_3 \tag{17}$$

$$p' = \frac{\sigma'_1 + 2\sigma'_3}{3}, \tag{18}$$

where ϵ_a and ϵ_r are the axial and radial strain, respectively.

The effect of the reinforcement on the shear strength was estimated by considering (i) reinforced soil analysed as a homogeneous composite material (Approach A), (ii) reinforced soil formed by two different materials (Approach B), and (iii) as soil having the same fundamental shear strength, with the effect of the reinforcement represented as an additional lateral or confining stress (Approach C). For Approach A, the shear strength of the reinforced soil was characterised by means of the apparent cohesion c'_r (Eq. 7) and the apparent friction angle ϕ'_r (Eq. 10). For Approach C, the shear strength was estimated according to the additional lateral confining stress $\Delta\sigma'_3$ (Eqs. 8 and 9) [11], as a function of

the increment of major principal stress $\Delta\sigma'_{\text{IfU-R}}$ (Eq. 2). For Approach B, this additional lateral confining stress was also expressed as an interface friction angle δ (Eq. 11) and an interface efficiency R_{int} (Eq. 2).

Statistical Analysis

Analysis of Covariance (ANCOVA) was used to make inferential comparisons for the linear relation between t and s' considering different specimen diameters (*D70* and *D150*). This analysis combines the ideas of the LRA with those of the Analysis of Variance (ANOVA) to compare several regression models (t as a function of s'), each associated with a category of the factor under analysis (type of specimen, *D70* and *D150*). For non-cohesive soils, the ANCOVA model can be formalized as the multivariate linear regression model

$$t_i = \sin(\phi')s'_i + zs'_ix_i + u_i, \tag{19}$$

where (t_i, s'_i) , $i = 1, 2, \dots, n$ are the n pairwise experimental observations, being t and s' , respectively, the dependent and independent variables of the model. This formalization adopts the additional binary variable $x = \{0, 1\}$ to code the belonging of a given observation i to the independent group (either *D150* or *D70*) as well as a joint term z (also known as a statistical interaction) to investigate whether the covariates s' and x exhibit a significant joint effect on t . Briefly, a null joint term z implies that the slope of s' on t is $\sin\phi'$, regardless of the group x . Finally, u is the unobserved error term of the model, which is used to evaluate the amount by which the model may differ from the empirical data. The regression parameters $\sin\phi'$ and z are estimated from the experimental data by least-squares minimization, i.e., by minimizing the sum of the squared differences between the actual observed responses and their values predicted by the optimal model. The corresponding p values were used to inspect the statistical significance of the coefficients at a significance level $\alpha = 5\%$. The effect of specimen size was also quantified to give the amount of variance of t that is explained by each term in the linear model. In the presence of a statistically non-significant joint term z (i.e., one cannot reject the null hypothesis that z is equal to zero), the linear model in Eq. 19 simplifies to

$$t_i = \sin(\phi')s'_i + u_i, \tag{20}$$

which highlights that the slope $\sin\phi'$ is the same for both *D70* and *D150* specimens. In such case, the linear model in Eq. 20 was re-estimated in a twofold manner, by considering $n = 12$ observations (*D70* + *D150* specimens) or $n = 9$ observations from the *D70* specimens alone. This analysis allows the comparison of these approaches in the quantification of ϕ' , specifically to identify the approach leading to a friction

angle of the safe side. Using this method for R specimens corresponds to Approach A.

The ANCOVA procedure was repeated for the specimens without and with reinforcement (U and R , respectively) to provide insights into the influence of the reinforcement on the relation between t and s' when taking into account the different specimen diameters (Table 1). ANCOVA was also used to analyse the two different failure envelopes at peak stress ratio and at the end of the test. The friction angles (peak and end of test) obtained by the univariate linear regression model are later compared with those obtained by the multivariate linear regression model.

All statistical procedures were implemented in Microsoft Excel version 2021 and the statistical software IBM-SPSS version 29.

Results and Discussion

Summary of Results

Figure 6 shows the mobilised angle of friction ϕ'_{mob} and the volumetric strain ϵ_{vol} plotted against the triaxial shear strain ϵ_s , obtained from small ($D70$) and large ($D150$) specimens of unreinforced (U) and reinforced (R) soils. The responses for $D70$ and $D150$ specimens were qualitatively different. For the U soil, the mobilised angle of friction ϕ'_{mob} for the $D70$ specimens exhibited strain hardening until a peak strength

was reached, followed by strain softening until the end of the test. After some initial contraction, the volumetric strain became negative and the $D70$ specimens exhibited dilation. On the other hand, the $D150$ response was characterised by strain hardening until the end of the test, with no clear intermediate peak; the volumetric strains were mostly contractile. As there was no evidence of the specimens reaching critical state, the results at the end of the test were not designated as such, for either $D70$ or $D150$.

The inclusion of a reinforcement layer led to an improved response, with higher mobilised friction angles ϕ'_{mob} than to the corresponding unreinforced specimens. A more detailed discussion is given in the following sections.

In the following sections, the discussion of the test results (Table 2) is grouped according to the type of analysis carried out: shear strength analysis (described in Sect. 2.1) and statistical analysis (Sect. 2.2). For the shear strength analysis, the results for $D70$ specimens were considered using the average result for the three specimens tested at each different value of confining stress; thus, for both $D70$ and $D150$, one set of results per confining stress is available. For the statistical analysis, all the data were used to define the failure envelopes, i.e., for the statistical analysis, all sets of data were considered separately.

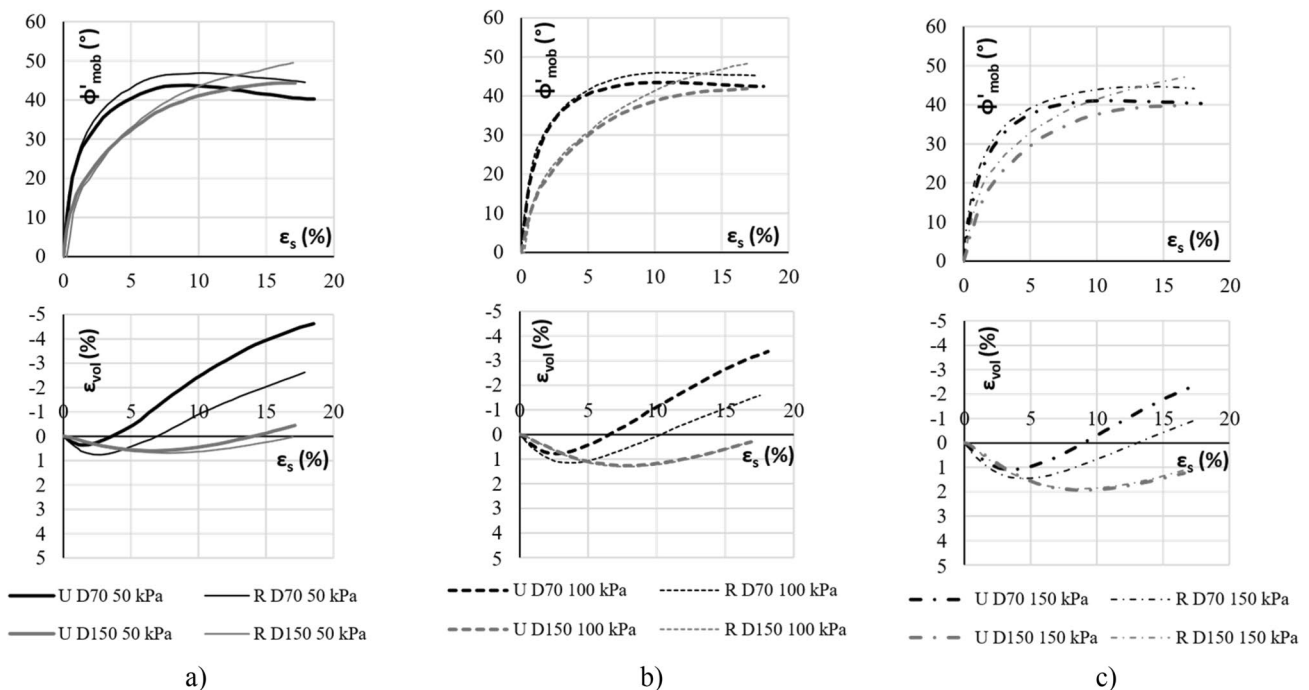


Fig. 6 Triaxial tests results (mobilised angle of friction ϕ'_{mob} and volumetric strain ϵ_{vol} versus triaxial shear strain ϵ_s), for different sized specimens (diameters 70 and 150 mm), one specimen per confining pressure: **a** 50 kPa; **b** 100 kPa; **c** 150 kPa

Table 2 Summary of the triaxial tests results in terms of minor (σ'_3) and major (σ'_1) principal stresses and stress ratio q/p' for *U D70* and *R D70* (3 specimens per confining stress) and *U D150* and *R D150* (1 specimen per confining stress) at the peak and at the end of the test ($\epsilon = 17\%$)

| Stress state | σ'_3 | Specimen | | | | | | | | |
|--------------|--------------------------------|--------------|--------|---------------|--------|--------------|--------|---------------|--------|------|
| | | <i>U D70</i> | | <i>U D150</i> | | <i>R D70</i> | | <i>R D150</i> | | |
| | | 9 tests | | 3 tests | | 9 tests | | 3 tests | | |
| | | σ'_1 | q/p' | σ'_1 | q/p' | σ'_1 | q/p' | σ'_1 | q/p' | |
| | (kPa) | (kPa) | (-) | (kPa) | (-) | (kPa) | (-) | (kPa) | (-) | |
| Peak | 50 | 269.69 | 1.78 | 281.95 | 1.82 | 313.88 | 1.91 | 376.21 | 2.06 | |
| | 100 | 534.27 | 1.77 | 502.01 | 1.72 | 603.80 | 1.88 | 687.69 | 1.99 | |
| | 150 | 736.98 | 1.70 | 685.84 | 1.63 | 849.63 | 1.83 | 971.62 | 1.94 | |
| | 50 | 266.82 | 1.77 | – | – | 321.88 | 1.93 | – | – | |
| | 100 | 541.54 | 1.79 | – | – | 607.84 | 1.89 | – | – | |
| | 150 | 725.31 | 1.68 | – | – | 854.97 | 1.83 | – | – | |
| | 50 | 274.99 | 1.80 | – | – | 320.86 | 1.93 | – | – | |
| | 100 | 540.52 | 1.78 | – | – | 612.95 | 1.89 | – | – | |
| | 150 | 724.29 | 1.68 | – | – | 858.06 | 1.83 | – | – | |
| | End of test, $\epsilon = 17\%$ | 50 | 194.59 | 1.46 | 281.95 | 1.82 | 263.88 | 1.74 | 376.21 | 2.06 |
| | | 100 | 446.46 | 1.60 | 502.01 | 1.72 | 557.07 | 1.81 | 687.69 | 1.99 |
| | | 150 | 614.45 | 1.52 | 685.84 | 1.63 | 837.24 | 1.81 | 971.62 | 1.94 |
| 50 | | 213.56 | 1.56 | – | – | 296.29 | 1.86 | – | – | |
| 100 | | 449.48 | 1.61 | – | – | 576.16 | 1.84 | – | – | |
| 150 | | 579.18 | 1.46 | – | – | 845.76 | 1.82 | – | – | |
| 50 | | 232.97 | 1.65 | – | – | 285.07 | 1.83 | – | – | |
| 100 | | 514.91 | 1.74 | – | – | 589.42 | 1.86 | – | – | |
| 150 | | 698.74 | 1.65 | – | – | 838.63 | 1.81 | – | – | |

Shear Strength Analysis

The stress ratio q/p' (Table 2) shows that the mobilised shear strength of the reinforced soil was greater than for the unreinforced soil tested under similar conditions. As critical states were not reached, a critical state parameter could not be determined from the stress ratio (q/p') data. The contribution of the reinforcement to the overall strength increase is likely to be due to mobilisation of frictional forces at the soil–geosynthetic interface and tensile forces associated with the load–strain response of the geosynthetic, as the reinforcement extends during loading. Quantifying the contribution of the load–strain response of the geosynthetic is difficult, as the extensions of the reinforcement cannot be determined from triaxial test boundary measurements.

The results also show (Fig. 6) that the presence of the layer of reinforcement leads to higher mobilised resistance (represented by ϕ'_{mob}) and reduced dilatancy relative to the corresponding unreinforced response (*D70* and *D150*), except for the *R D150* specimens tested at higher confining stress (i.e., 100 kPa and 150 kPa). For these *R D150* specimens, the volumetric strains were similar to the corresponding unreinforced specimens, despite the higher resistance observed. Two effects can be responsible for the

restricted dilatancy. First, the presence of a disc of reinforcement at mid-height of the specimen (with a continuous, sheet structure) prevents soil particles from moving vertically at that position, thus, decreasing the volumetric strains of the reinforced soil. Secondly, the mobilisation of shear stresses on the soil–geosynthetic interface restrains radial strains of the specimen and, consequently, also its volumetric strains.

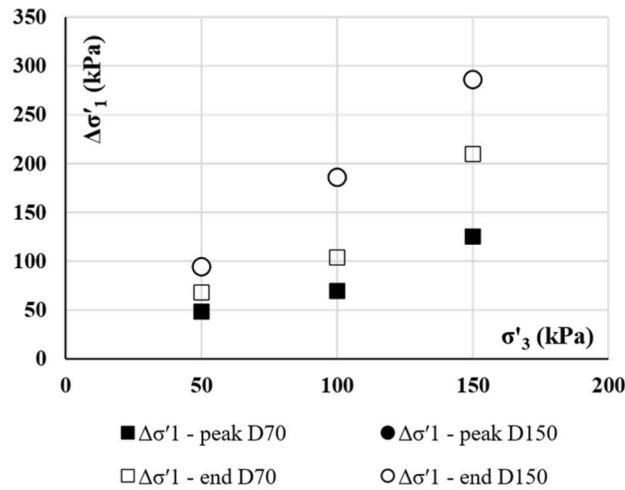
The stress ratio q/p' (Table 2) is greater for the large specimens (*D150*) than for the small (*D70*), except for the peak data of unreinforced specimens (*U*). The same trend, of larger specimens having higher strengths, was observed by Markou and Droudakis [19]. Testing larger specimens mobilizes more grains at a given applied stress, allowing better (more uniform) distribution of stresses within the soil skeleton and rearrangement of soil particles. This effect will tend to be more significant at large deformations, when the overall movement of grains is larger (i.e., end of the test), than at the peak.

Table 3 summarises the results obtained for the shear strength of the reinforced soil and the soil–geosynthetic interface: increment of principal stress due to the introduction of the reinforcement $\Delta\sigma'_{IFR-U}$, Eq. 3; additional lateral confining stress $\Delta\sigma'_3$, Eq. 8 by Gray et al. [7], and Eq. 9 by Yang [11] (Approach C); apparent cohesion c'_s , Eq. 7 (Approach A); apparent friction angle ϕ'_s , Eq. 10 (Approach

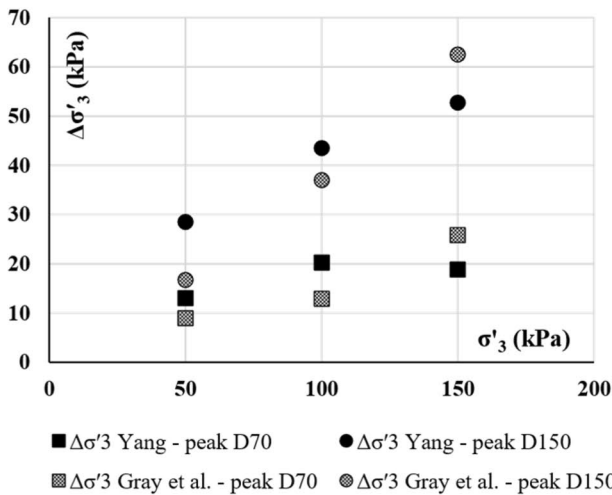
Table 3 Shear strength of the reinforced soil and the soil–geosynthetic interface: confining stress σ_3 ; increment of principal stress due to the introduction of the reinforcement $\Delta\sigma'_{IU-R}$; additional lateral confining stress $\Delta\sigma'_3$; apparent cohesion c'_r ; apparent friction angle ϕ'_r ; friction angle of the interface δ ; interface efficiency factor R_{int}

| Stress state | Specimen | σ'_3 (kPa) | $\Delta\sigma'_{IU-U}$ Equation 3 (kPa) | $\Delta\sigma'_3$ Yang [11] Equation 9 (kPa) | $\Delta\sigma'_3$ Gray et al [7] Equation 8 (kPa) | ϕ'_r Equation 10 (°) | c_r Equation 7 (kPa) | δ Equation 11 (°) | ϕ'_{mobU} Equation 15 (°) | R_{int} Equation 2 (-) |
|--------------------------------|----------|----------------------|---|--|---|---------------------------------|------------------------------|--------------------------------|--------------------------------------|--------------------------------|
| Peak | R D70 | 50 | 48.4 | 13.0 | 8.9 | 46.8 | 8.5 | 9.6 | 43.5 | 0.2 |
| | | 100 | 69.4 | 20.2 | 12.9 | 45.9 | 12.8 | 7.2 | 43.4 | 0.1 |
| | | 150 | 125.4 | 18.8 | 25.8 | 44.5 | 24.8 | 10.3 | 41.2 | 0.2 |
| End of test, $\epsilon = 17\%$ | R D150 | 50 | 94.3 | 28.5 | 16.7 | 49.9 | 13.7 | 14.9 | 44.3 | 0.3 |
| | | 100 | 185.7 | 43.5 | 37.0 | 48.3 | 29.6 | 17.9 | 41.9 | 0.4 |
| | | 150 | 285.8 | 52.7 | 62.5 | 47.1 | 48.3 | 21.1 | 39.9 | 0.5 |
| End of test, $\epsilon = 17\%$ | R D70 | 50 | 68.0 | 14.3 | 15.9 | 44.3 | 12.6 | 18.7 | 38.2 | 0.4 |
| | | 100 | 103.9 | 31.0 | 22.1 | 44.7 | 18.9 | 13.0 | 40.4 | 0.3 |
| | | 150 | 209.8 | 41.8 | 49.9 | 44.2 | 39.2 | 19.6 | 44.2 | 0.5 |
| End of test, $\epsilon = 17\%$ | R D150 | 50 | 94.3 | 28.5 | 16.7 | 49.9 | 13.7 | 14.9 | 44.3 | 0.3 |
| | | 100 | 185.7 | 43.5 | 37.0 | 48.3 | 29.6 | 17.9 | 41.9 | 0.4 |
| | | 150 | 285.8 | 52.7 | 62.5 | 47.1 | 48.3 | 21.1 | 39.9 | 0.5 |

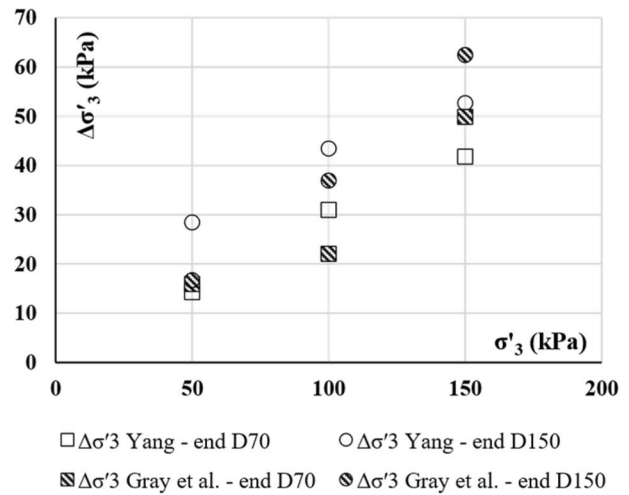
The mobilised friction angle for the corresponding unreinforced soil specimen ϕ'_{mobU} is included



a)



b)



c)

Fig. 7 Effect of the reinforcement as (Approach C): **a** increment of major principal stress ($\Delta\sigma'_{1FR-U}$) for specimens with different dimensions (*D70* and *D150*), peak and end of the test; additional lateral

confining stress ($\Delta\sigma'_3$) obtained with two different proposals (Yang, Eq. 9, and Gray et al., Eq. 8) and specimen sizes (*D70* and *D150*), **b** peak and, **c** end of the test

A); friction angle of the interface δ , Eq. 11 (Approach B); interface efficiency factor R_{int} , Eq. 2 (Approach B).

Figure 7a summarises the increment of the major principal stress due to the introduction of the reinforcement, $\Delta\sigma'_{1FR-U}$, for specimens of different sizes (*D70* and *D150*), for the peak and at the end of the test. As expected, at the end of the test, the larger specimens (*D150*) are associated with a greater stress increment than the small specimens (*D70*). For *D70*, $\Delta\sigma'_{1FR-U}$ was greater at the end of the test than at the peak. This reflects higher levels of mobilisation of the reinforcement and of the soil–geosynthetic interface strength, as the specimen is sheared and strains increase.

The additional lateral confining stress $\Delta\sigma'_3$ (Approach C) due to the reinforcement obtained from Eq. 8 by Gray

et al. [7] and Eq. 9 by Yang [11] is different (Fig. 7b and c): up to a confining stress of 100 kPa, the method proposed by Yang [11] leads to higher values of $\Delta\sigma'_3$ (except for *R D70* at 50 kPa); for a confining stress of 150 kPa, the opposite trend is observed. The difference between $\Delta\sigma'_3$ values at peak and at the end of the test (*D70*) tends to increase with increasing confining stress (Table 3). The $\Delta\sigma'_3$ values at the end of the test obtained using the two equations are closer than at the peak (*D70*) (Table 3 and Fig. 7). Regardless of the procedure used to estimate $\Delta\sigma'_3$, a larger specimen size (*D150*) leads to a higher lateral confining stress.

Assuming the reinforced soil (*R*) has the same grain-to-grain shear strength as the soil (*U*), the principal stress

increments due to the reinforcement $\Delta\sigma'_3$ and $\Delta\sigma'_{1fR-U}$ must be considered simultaneously, as they represent a translation of the Mohr circle towards higher normal stresses (Approach C). These increments can be related via Eq. 21 and the angle of friction of the soil (ϕ'), which can be obtained from Eq. 9 due to Yang [11], where $K_a = 1/K_p$. Thus, the stress increments $\Delta\sigma'_3$ and $\Delta\sigma'_{1fR-U}$ increase simultaneously, as evident from

$$\Delta\sigma'_3 = K_a \Delta\sigma'_{1fR-U} \tag{21}$$

The shear strength of the reinforced soil may be represented by an apparent friction angle ϕ'_r (Fig. 8a) and no cohesive intercept ($c' = 0$ kPa), assuming the reinforced soil behaves as a single homogeneous material (Approach A). Although Eq. 10 was proposed for the peak response, it was also used in this paper for the end-of-test data. As expected, the peak values are larger than those at the end of the test (D70); that difference tends to decrease with increasing confining stress. This result reflects the inhibition of dilatancy associated with a higher confining stress, suppressing the peak strength (as schematically represented in Fig. 3).

The apparent friction angle ϕ'_r (Approach A) decreases with increasing confining stress, for both peak and end of the test, except for R D70 at the end of the test (Table 3). This trend could be interpreted as a reduction of the influence of the reinforcement with increasing confining stress. However, this is again consistent with the inhibition of dilatancy associated with the reinforcement and a higher confining stress. The estimates of ϕ'_r (Eq. 10) coincide with the value of ϕ'_{mob} (Eq. 15) obtained for the reinforced specimens. This is to be expected, as Eq. 9 for ϕ'_r (Higuchi et al. [9]) and Eq. 15 for ϕ'_{mob} are the same.

The apparent cohesion c'_r (Approach A) (Eq. 8, Gray et al. [7]), illustrated in Fig. 8b, increases with increasing confining stress and is larger for the end of the test data than for the corresponding peak. The apparent cohesion is proportional to the additional lateral confining stress $\Delta\sigma'_3$ (Eq. 8, Gray et al. [7]). As discussed previously, a strength parameter properly associated with cementation has no physical meaning and should be avoided.

Alternatively, the contribution of the reinforcement to the shear strength of the reinforced soil may be estimated as an interface friction angle δ , obtained from Eq. 11 (Approach B). This equation assumes that interface friction is the same on both faces of the reinforcement, and along all radius (corresponding to an average response), it also includes the contribution of the extension of the reinforcement.

For the larger specimens (D150), the interface angle of friction (which is calculated to be the same at both the peak and at the end of the test) is directly proportional to the confining stress applied during the triaxial test. For smaller specimens (D70), no clear trend is observed when analysing the influence of the confining stress (Fig. 9). Nevertheless, as expected, for a particular confining stress, the interface friction mobilised at the end of the test is larger than for the peak (D70).

The interface efficiency factor R_{int} (Approach B) (Table 3) is always smaller than 1, as expected for a sheet reinforcement. However, the values are much smaller (0.1–0.5) than are often reported in the literature (0.6–1.0) [3]. The main reason for this is the test method and the associated relative movement between the soil and the geosynthetic along their interface. The range of values usually reported in the literature refers to data from direct shear and pull-out tests, where the relative displacements along the soil–geosynthetic

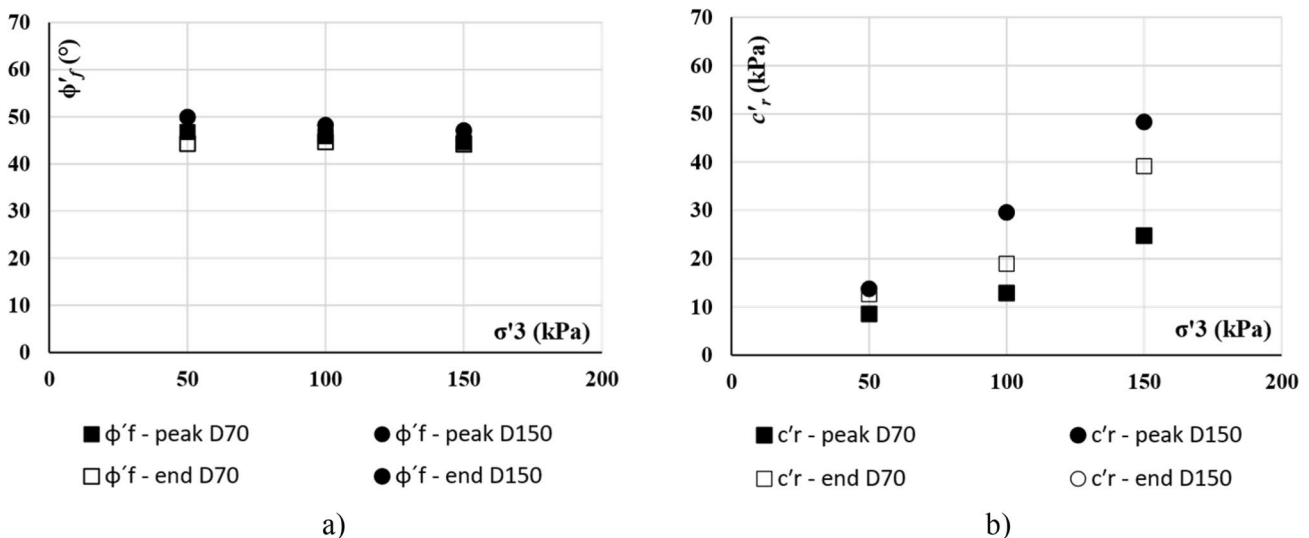


Fig. 8 Effect of the reinforcement considering the reinforced soil as a single homogeneous material (Approach A): **a** apparent friction angle of the reinforced soil ϕ'_r , Higuchi et al. [9] **b** apparent cohesion of the reinforced soil c'_r , Gray et al. [7]

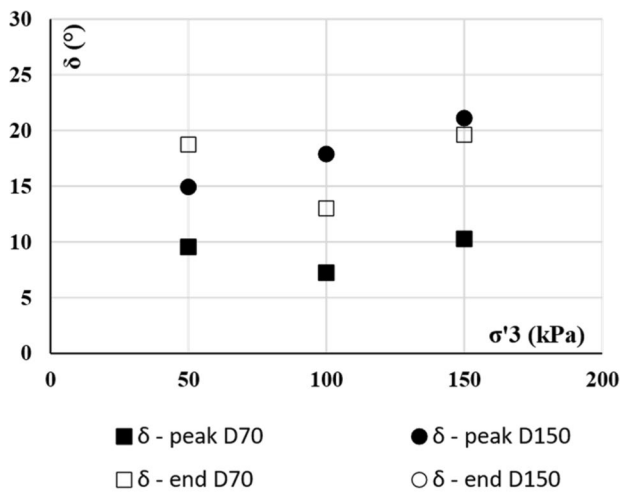


Fig. 9 Interface friction angle δ (Approach B), Markou [13]

interface are much larger than in triaxial tests. For example, in pull-out tests the displacement along the soil–reinforcement contact can reach 25–50 mm, depending on the type of geosynthetic [24, 25]. In the triaxial tests reported herein, the upper limit of the soil–geosynthetic relative displacement corresponds to the maximum radial displacement of *R D150* specimens for similar confining stress (50 kPa), which was 6 mm. Because of that, the shear strength mobilised at the soil–geosynthetic interface in triaxial loading is smaller than for direct shear and pull-out conditions.

Comparing data for *D70* and *D150*, in most cases, the larger specimens (*D150*) gave larger values of R_{int} , due to the associated greater radial displacements at the specimen mid-height. The values at the end of the test tend to be closer than those at peak (*D70*).

Some authors [26] have shown that, if the effect of the fibre reinforcement can be isolated, the shear strength of fibre-reinforced soil (with randomly distributed fibres) can be represented by the critical state framework for the unreinforced soil. This approach should be extended to the case of horizontal reinforcement. However, there are some challenges. In particular, quantifying the contribution of the load–strain response of the geosynthetic to the enhanced response is difficult—the only data available relate to the in-isolation load–strain response of the geosynthetic, and the

actual extensions of the reinforcement cannot be measured from the triaxial test results.

Statistical Analysis

ANCOVA was based on a regression model of t on s' built from the data presented in Table 2, with the aim of comparing specimens of different sizes, without and with reinforcement. Table 4 summarises the parameter estimates, p values, and the effect size associated with each term of the regression model. The results demonstrate that the triaxial test results obtained from unreinforced specimens of different diameter (*U D70* and *U D150*) can be characterised using the same failure envelopes at both the peak and at the end of the test. For the reinforced specimens (*R D70* and *R D150*), triaxial results can be characterised using the same failure envelope only at the end of the test.

For the unreinforced specimens, the joint term in the regression model is not statistically significant for the peak (p value = 0.124) or for the end of the test (p value = 0.669), thus, suggesting that the failure envelopes obtained using different specimen sizes of unreinforced specimens have no significant difference. This means that there is no statistical reason to reject the null hypothesis, $H_0: z=0$ at 5% significance level. Geotechnically, the null hypothesis is: *D70* and *D150* specimens have the same friction angle, for 5% of significance. For the reinforced specimens, the joint term is significant for the failure envelope at peak states (p value = 0.019). Thus, the failure envelopes obtained from different specimen sizes are statistically different. Nevertheless, by the end of the test, this joint term is not statistically significant (p value = 0.165), which indicates that the envelopes obtained from the two different specimen sizes are similar. This observation supports the idea that in the case of reinforced soil characterisation, in addition to the scaling rules that need to be met, the mechanical properties should be evaluated at the end of the test. This should whenever possible be the critical state. The lack of statistical similarity between the reinforced soil envelopes, for different specimen sizes, at peak states shows that the traditional criterion for selecting the required diameter of a triaxial specimen based on D_{max} of the soil only is not sufficient. Nonetheless, the statistical similarity between reinforced and unreinforced specimens, for different specimen sizes, at large deformations supports the decision not remove the larger particles when

Table 4 ANCOVA results (parameter estimate, p value, and effect size) for *U* and *R* soils, considering peak failure envelope without cohesion and end of the test failure envelope

| Stress state | Parameter | <i>U</i> | | | <i>R</i> | | |
|--------------|-------------|------------------|-----------|-------------|------------------|-----------|-------------|
| | | Analytical value | p value | Effect size | Analytical value | p value | Effect size |
| Peak | $\sin\phi'$ | 0.604 | <0.01 | 0.990 | 0.713 | <0.01 | 0.999 |
| | z | 0.040 | 0.124 | 0.269 | -0.027 | 0.019 | 0.520 |
| End of test | $\sin\phi'$ | 0.604 | <0.01 | 0.952 | 0.713 | <0.01 | 0.999 |
| | z | 0.024 | 0.669 | 0.024 | -0.015 | 0.165 | 0.226 |

testing *D70* specimens. Another important aspect is that unreinforced failure envelopes (the regressions) are more similar for the end-of-test than for the peak results. The joint term, z , exhibits higher p values, which suggests less evidence against the null hypothesis ($h_0: z = 0$) as opposed to the bilateral alternative hypothesis (i.e., *D70* and *D150* specimens do not have the same friction angle for 5% of significance). This is expected as the soil is about to reach a critical state, which for a given soil is independent of internal and external conditions (e.g., particle arrangement/density, confining stress, and potentially specimen size). Conversely, the peak state depends on these factors. For this reason, it is to be expected that peak results obtained from tests on different sized specimens result in less similar failure envelopes. This is a further reason for not using peak strengths or responses in design.

Once it has been demonstrated that the joint term is not significant, it can be concluded that the slope of the failure envelope, $\sin\phi'$, is fairly similar regardless of the group (*D70* or *D150*) at 5% significance level. For this reason, for the unreinforced specimens at peak and at the end of the test, and for reinforced specimens at the end of the test, the regressions were re-estimated with the 12 observations; results are presented in Table 5. The friction angle was then evaluated from these models, with the aim of assessing whether it changes significantly when considering only the *D70* or both *D70* and *D150* specimens.

Table 6 presents the results obtained for the various cases. It demonstrates that the *D70* plus *D150* observations for the *U* specimens generate failure envelopes (for both the peak and the end of the test) with more conservative friction angles. Hence, using results obtained from tests on the different specimen sizes for unreinforced soils to generate the failure envelope errs on the safe side. At this point, it is important to recall that this assumes that the joint term is not statistically significant. For the *R* specimens, the friction angle obtained from *D70* and *D150* tests is practically the same as that obtained from the *D70* specimens alone; 44.5° and 44.4° , respectively (Table 6). For this reason, considering *D70* plus *D150* observations to generate reinforced soil failure envelopes is still valid and on the safe side.

Conclusions

In this paper, triaxial test data of a soil reinforced with a geosynthetic, and specimens with different dimensions (diameters 70 and 150 mm) were used to assess changes in shear strength and to carry out a statistical analysis. The applications of

Table 6 Friction angle of the soil considering *D70* observations or both *D70* and *D150* observations (*D70*+*D150*)

| Specimen | No. of specimens | Stress state | ϕ' (°) |
|--------------------------|------------------|-----------------------------------|--------------|
| <i>U</i> | | | |
| <i>D70</i> | 9 | Peak | 42.1 |
| | | End of the test $\epsilon = 17\%$ | 38.9 |
| <i>D70</i> + <i>D150</i> | 12 | Peak | 39.5 |
| | | End of the test $\epsilon = 17\%$ | 38.5 |
| <i>R</i> | | | |
| <i>D70</i> | 9 | Peak | 45.1 |
| | | End of the test $\epsilon = 17\%$ | 44.4 |
| <i>D70</i> + <i>D150</i> | 12 | Peak | ^a |
| | | End of the test $\epsilon = 17\%$ | 44.5 |

^aFor this stress state, *D70* and *D150* slopes are less similar

geosynthetics targeted include transportation infrastructure, where the loading is closely axisymmetric. The increases in shear strength of the reinforced soil and of the soil–geosynthetic interface were analysed using equations from the literature, with three different approaches. Approach A considers the reinforced soil as a homogeneous material with strength parameters similar to those of a soil (cohesion intercept and angle of friction); Approach B considers the reinforced soil as two different materials; Approach C considers the influence of the reinforcement as a confining stress while representing the reinforced soil as soil having the same fundamental shear strength. The difference between the triaxial results obtained from specimens of different sizes was assessed using ANCOVA. When the joint term of the regression model was not statistically significant, the characterisation from different specimen sizes was used to generate soil failure envelopes. The main conclusions from this study are as follows:

1. The inclusion of a horizontal layer of geosynthetic reinforcement at mid-height of triaxial specimens results in an increased shear strength (~29% for smaller specimens; ~46% for larger specimens) and suppressed dilatancy, particularly at lower confining stress.
2. The interface efficiency factor obtained under conventional triaxial loading (0.1–0.5) is smaller than for direct shear and pull-out conditions (0.6–1.0), owing to differences in the soil–geosynthetic relative movement along their interface. Thus, when choosing a method to characterise soil reinforced with geosynthetics, the type of

Table 5 Univariate linear regression model built on the stress space (s' , t) with *D70* and *D150* observations: peak failure envelope without cohesion and end of the test failure envelope

| Stress state | Parameter | <i>U</i> | | | <i>R</i> | | |
|--------------|-------------|------------------|-----------|-------------|------------------|-----------|-------------|
| | | Analytical value | p value | Effect size | Analytical value | p value | Effect size |
| Peak | $\sin\phi'$ | 0.636 | <0.01 | 0.977 | – | – | – |
| End of test | $\sin\phi'$ | 0.622 | <0.01 | 0.989 | 0.701 | <0.01 | 1.000 |

loading and the failure mechanics should be taken into consideration.

3. Using the equations from the literature, Approach A led to unsafe strength parameters, in that the apparent cohesion does not exist. The use of a cohesion intercept with no physical meaning is misleading and must be avoided, for both unreinforced and reinforced soil. For the case of triaxial conditions, Approach B needs to be further explored. The interface angle of friction can be used to represent the shear strength of the soil–geosynthetic interface under specific conditions. Most geosynthetics are orthotropic, with two perpendicular directions of higher strength; the triaxial test setup allows assessment of the average response along different radii of the reinforcement relative to the axis of the specimen (along which the loading is applied). Approach C is also limited, as the effect of the reinforcement is represented indirectly; the additional confining stress is the basis for quantifying the parameters in Approaches A and B.
4. Statistical analysis at the 5% significance level supports the hypothesis that the failure envelopes of the unreinforced soil obtained from tests on two different specimen sizes (diameters 70 and 150 mm) are not significantly different, particularly for large deformations as the critical state of the soil is approached. For the reinforced soil, the specimen size did not influence the failure envelope at large deformations, but influenced the peak state (5% significance level). Thus, it is evident that the peak response depends on the specimen dimensions.
5. When planning triaxial tests on reinforced soil, the traditional criterion for selecting the required specimen diameter based on the maximum particle size of the soil is not sufficient for analysing the peak response. At peak, the response is dependent on internal and external conditions (e.g., particle arrangement/density, confining stress, and potentially specimen size).
6. For large deformations (as critical state is approached), the combination of the results obtained with different triaxial specimen sizes led to a unique failure envelope that was conservative. For the reinforced specimens, the friction angle obtained from specimens of different dimensions is identical to that obtained from the smaller specimens only (44.5°). Further validation is needed, including more soils and reinforcement types and more detailed observations.

The results and discussion presented herein highlight the need to develop a sound framework for assessing the shear strength of reinforced soil as a composite material. This should be based on the stress–strain response of each

material, soil matrix and reinforcement elements, and their interaction mechanisms, represented realistically.

Acknowledgements Rafael Anjos was supported by the doctoral Grant PRT/BD/154385/2022 financed by Portuguese Foundation for Science and Technology (FCT), and with funds from European Social Fund (ESF) and Por_Centro Program, under MIT Portugal Program. The financial support of FCT (“Fundação para a Ciência e Tecnologia”—Portugal) is gratefully acknowledged through the project UIDB/04450/2020 (RISCO) and UIDB/00127/2020 (IEETA, www.ieeta.pt). This work was financially supported by the project TRANSFORM funded by the Portuguese Resilience Plan (PRR) through European Union—NextGenerationEU.



Author contributions Conceptualization: RA, SG, and MP-L. Data curation: RA, DMC, and MP-L. Formal analysis: RA, DMC, and MP-L. Funding acquisition: RA, DMC, SG, MP-L, and WP. Investigation: RA and DMC. Methodology: RA, SG, and MP-L. Project administration: SG and MP-L. Resources: DMC, SG, and MP-L. Supervision: SG, MP-L, and WP. Validation: RA, DMC, SG, MP-L, and WP. Visualization: RA, SG, and MP-L. Writing—original draft: RA, SG, and MP-L. Writing—review and editing: RA, DMC, SG, MP-L, and WP.

Funding Open access funding provided by FCTIFCCN (b-on). The authors declare that they have no known competing financial interests or personal relationships that could have appeared to influence the work reported in this paper.

Availability of data The data presented in this study are available on request from the corresponding author.

Declarations

Conflict of interest Margarida Pinho-Lopes is a member of the editorial board of the International Journal of Geosynthetics and Ground Engineering. She was not involved, at any stage, with handling nor peer review of the paper.

Open Access This article is licensed under a Creative Commons Attribution 4.0 International License, which permits use, sharing, adaptation, distribution and reproduction in any medium or format, as long as you give appropriate credit to the original author(s) and the source, provide a link to the Creative Commons licence, and indicate if changes were made. The images or other third party material in this article are included in the article's Creative Commons licence, unless indicated otherwise in a credit line to the material. If material is not included in the article's Creative Commons licence and your intended use is not permitted by statutory regulation or exceeds the permitted use, you will need to obtain permission directly from the copyright holder. To view a copy of this licence, visit <http://creativecommons.org/licenses/by/4.0/>.

References

- Jewell RA (1996) Soil reinforcement with geotextiles, vol 123. Construction Industry Research and Information Association, London
- Salgado R (2020) Forks in the road: rethinking modeling decisions that defined the teaching and practice of geotechnical engineering. In: International conference on geotechnical engineering education 2020 (GEE2020), pp 51–68. <https://www.issmge.org/education/recorded-webinars/forks-in-the-road-rethinking-modeling-decisions-that-defined-teaching-and-practice-of-geotechnical-engineering>. Accessed 28 Jun 2023
- Lopes ML (2015) Soil-geosynthetic interaction. In: Shukla SK (ed) Geosynthetics and their applications, 2nd edn. Thomas Telford, London, pp 45–66
- Lees AS (2017) Simulation of geogrid stabilisation by finite element analysis. In: 19th International conference on soil mechanics and geotechnical engineering. pp 1377–1380
- Saez J (1997) Caracterización geomecánica de geotextiles [in Spanish]. Curso sobre técnicas generales de refuerzo del terreno y sus aplicaciones. Centro de estudios y experimentación de obras públicas (CEDEX), Madrid
- Carlos DM, Pinho-Lopes M, Lopes ML (2018) Stress–strain response of sand reinforced with a geocomposite. In: 11th International conference on geosynthetics. pp 1091–1098
- Gray DH, Asce AM, Al-Refeai T (1986) Behavior of fabric—versus fiber-reinforced sand. *J Geotech Eng* 112(8):804–820
- Schlosser F, Long NT (1974) Recent results in french research on reinforced earth. *J Constr Div* 100:223–237
- Higuchi T, Ishihara K, Tsukamoto Y, Masuo T (1998) Deformation and strength of geogrid-reinforced granular soil at plane strain conditions. *Soils Found* 38(1):221–227
- Bathurst RJ, Karpurapu R (1993) Large-scale triaxial compression testing of geocell-reinforced granular soils. *Geotech Test J* 16(3):296–303. <https://doi.org/10.1520/gtj10050j>
- Yang Z (1972) Strength and deformation characteristics of reinforced sand. University of California
- Ruiken A, Ziegler M, Vollmert L, Duzic I (2010) Recent findings about the confining effect of geogrids from large scale laboratory testing. In: 9th International conference on geosynthetics
- Markou IN (2018) A study on geotextile—sand interface behavior based on direct shear and triaxial compression tests. *Int J Geosynthet Ground Eng*. <https://doi.org/10.1007/s40891-017-0121-7>
- Atmatzidis DK, Athanasopoulos GA, Papantonopoulos CI (1994) Sand-geotextile interaction by triaxial compression testing. In: 5th International conference on geotextiles, geomembranes and related products, Singapore, pp 377–380
- Broms BB (1988) Fabric reinforced retaining walls. In: International geotechnical symposium on theory and practice of earth reinforcement, pp 3–31
- Omar T, Sadrekarimi A (2015) Effect of triaxial specimen size on engineering design and analysis. *Int J Geo-Eng*. <https://doi.org/10.1186/s40703-015-0006-3>
- Lade PV (2016) Triaxial testing of soils, 1st edn. Wiley, Hoboken
- BS EN ISO 17892-8 (2018) Geotechnical investigation and testing - laboratory testing of soil
- Markou IN, Droudakis AI (2007) Behavior of reinforced sand: effect of triaxial compression testing factors. *New horizons in earth reinforcement*. CRC Press, Boca Raton, pp 569–575
- Handy RL (1981) Linearizing triaxial test failure envelopes. *Geotech Test J* 4(4):188–191. <https://doi.org/10.1520/GTJ10789J>
- Carlos DM (2016) Análise experimental e numérica do comportamento de estruturas de solo reforçado com geossintéticos: solo granular versus fino [in Portuguese]. University of Aveiro
- ASTM D2487-17 (2020) Standard practice for classification of soils for engineering purposes (unified soil classification system). <https://doi.org/10.1520/D2487-17E01>
- Wood DM (1984) On stress parameters. *Géotechnique* 34(2):282–287. <https://doi.org/10.1680/geot.1984.34.2.282>
- Pinho-Lopes M, Paula AM, Lopes ML (2015) Pullout response of geogrids after installation. *Geosynth Int* 22(5):339–354. <https://doi.org/10.1680/jgein.15.00016>
- Pinho-Lopes M, Paula AM, Lopes ML (2016) Soil–geosynthetic interaction in pullout and inclined-plane shear for two geosynthetics exhumed after installation damage. *Geosynth Int* 23(5):331–347. <https://doi.org/10.1680/jgein.16.00001>
- Ajayi O, Le Pen L, Zervos A, Powrie W (2017) A behavioural framework for fibre-reinforced gravel. *Geotechnique* 67(1):56–68. <https://doi.org/10.1680/JGEO.16.P.023>

Publisher's Note Springer Nature remains neutral with regard to jurisdictional claims in published maps and institutional affiliations.